

## **THRUST AUGMENTATION IN AN UNSTEADY SUPERSONIC EJECTOR**

Kathleen M. Tacina\*

National Aeronautics and Space Administration  
Glenn Research Center  
Cleveland, Ohio 44135, USA

Rene Fernandez\*

National Aeronautics and Space Administration  
Glenn Research Center  
Cleveland, Ohio 44135, USA

Stefanie M. Moody<sup>+</sup>

National Aeronautics and Space Administration  
Glenn Research Center  
Cleveland, Ohio 44135, USA

### **ABSTRACT**

An unsteady supersonic ejector with subsonic secondary flow was investigated experimentally. Thrust augmentation results for a primary flow Mach number of 3.7, secondary flow Mach numbers of 0.2 to 0.3, frequencies of 30 to 120 Hz, ejector length to nozzle diameter ratios  $L/d$  of 5.72 to 6.97, and a duty cycle (defined as pulse duration to total cycle duration) of 8% are presented. The thrust augmentation was found to be only weakly dependent on  $L/d$ , to increase with increasing frequency, to decrease with increasing secondary flow Mach number, and to increase with increasing pulse strength.

### **INTRODUCTION**

Pulsed ejectors may increase the thrust and reduce the noise in pulse detonation engines. In addition, past work<sup>1</sup> has shown that pulsed ejectors have higher thrust augmentation than do steady ejectors. However, the theory behind pulsed ejectors is not well understood and thus it is unclear how to design pulsed ejectors for maximum thrust augmentation. This study is designed to identify which parameters are important and how they affect the thrust augmentation of a pulsed ejector.

The design of pulsed ejectors is a complex problem; many parameters can affect ejector performance. These factors include: Mach number of the primary (nozzle) flow, Mach number of the secondary (ejector) flow, temperature/density ratio of the primary to secondary flow, pulse strength (defined as pressure amplitude), pulse shape, pulse rate, duty cycle (the ratio of pulse duration to cycle duration), ejector to nozzle area ratio, and ejector shape.

A series of complementary experiments conducted at NASA Glenn Research Center have examined factors that affect ejector performance. These experiments included: (1) a subsonic pulsejet-driven ejector<sup>2</sup>, (2) supersonic ( $M=2$ ) resonance tube driven ejectors<sup>3,4</sup>, (3) pulse detonation engine driven ejectors<sup>5</sup>, and (4) supersonic ( $M=3.7$  and  $M=5$ ) air-jet, nitrogen-jet, and helium-jet ejectors<sup>6</sup>. The experiments differ in what aspects of a pulse detonation engine they simulate, the parameters that are studied, and the type of measurements taken. This paper discusses the Fernandez supersonic jet-driven ejector experiment.

The purpose of this paper is to present the thrust augmentation results of this experiment as a function of pulse rate, pulse strength, ejector length to nozzle diameter ratio  $L/d$ , and secondary flow Mach number. The thrust was not measured directly but was instead calculated using data from a 17-probe total pressure rake.

### **EXPERIMENTAL SETUP**

In this experiment, a small nozzle placed on the centerline of the 1' x 1' supersonic wind tunnel (see Seablom et al<sup>7</sup> for a description of this facility) at NASA Glenn Research Center is pulsed at high frequency using a rotary valve system (see Figure 1 to 3). The nozzle simulates the primary exhaust flow from a pulse detonation engine (without hot or chemically reacting flow). Therefore, the rotary valve system is designed to produce a sharp pressure spike followed by a period of lower pressure. Figure 4 shows a typical graph of nozzle throat pressure versus time for a set of four pulses.

Three different nozzles – a Mach 5 air nozzle, a Mach 3.7 air nozzle, and a Mach 4.6 helium nozzle – are used. The valve system is designed to approximate the sharp pressure spikes of a pulse detonation engine (see Figure 3). The design of the valve system and nozzles is discussed in Fernandez et al<sup>6</sup>. The wind tunnel itself

---

\* AIAA member

<sup>+</sup> AIAA student member

This material is declared a work of the U.S. government and is not subject to copyright protection in the United States.

simulates an ejector with low speed secondary flow; therefore, it is run at a Mach number of 0.2-0.4.

Due to the velocity difference between the primary and secondary flows, there is mixed subsonic and supersonic flow in this experiment. The flow in the center of the wind tunnel test section downstream of the nozzle is supersonic while the pulse valve is open, but it is subsonic while the pulse valve is closed. In the rest of the test section, the flow is subsonic most of the time.

Four systems are used to take data. The ESCORT low frequency (1 reading/sec) central storage data recording system records steady state conditions and experimental parameters. The Datamax™ system records dynamic pressure data (sample rate: 100 kHz) from 41 high frequency transducers placed in the high pressure primary flow supply pipe, in static pressure taps on the tunnel walls, and on a 17-probe pitot rake downstream of the nozzle near the exit of the test section. The Phantom high speed (3,600 to 7,200 frames per second) digital camera records schlieren images that can be adjusted to show density gradients in either the horizontal or vertical directions. Finally, for a few cases, pressure sensitive paint on a test section side wall was used for flow visualization.

Figure 2 shows a schematic of the test section. The test section is 53.25 in long. As shown in this figure, the nozzle fairing intrudes into the wind tunnel nozzle block which is directly upstream of the test section. The sidewall dynamic pressure taps are at 8.65, 16.65, 24.65, 28.65, 32.65, 36.65, 40.65, and 44.65 in downstream of the test section entrance, the nozzle exit is at 29.5 in. The rake can be moved from 42.4 to 46.4 in downstream of the test section entrance.

The design of pulsed ejectors is a complex problem; many parameters can affect ejector performance. These factors include: Mach number of the primary (nozzle) flow, Mach number of the secondary (ejector) flow, temperature/density ratio of the primary to secondary flow, pulse strength (defined as the pressure entering the pulse valve system), pulse shape, pulse rate, duty cycle (the ratio of pulse duration to cycle duration), ejector to nozzle area ratio, and ejector shape. In this experiment, the pulse rate, pulse strength, duty cycle, Mach number of the primary and secondary flow, ejector to nozzle area ratio, and density ratio are varied (see Table 1). Only a subset of the data from this experiment is examined in this paper. The conditions used in this paper are given in italics in Table 1.

Primary flow Mach number	3.7, 4.6, 5
Secondary flow (tunnel) Mach number	0.2, 0.3
Pulse rate (Hz)	0, 30, 60, 80, 100, 120
Duty cycle (%)	8, 11, 16
Pulse strength, defined as pressure fed to pulse valve (psia)	300, 460, 520
Secondary:Primary Area Ratio	10, 31.2
Gas for primary flow	Air, Helium, Nitrogen
Gas for secondary flow	Air
Ejector length to nozzle diameter, L/d	5.72, 6.14, 6.97

**Table 1:** Experimental parameters.

### **DATA ANALYSIS**

This paper examines the thrust augmentation of the pulsed ejector as a function of secondary flow Mach number, pulse rate, pulse strength, and duty cycle for a primary flow Mach number of 3.7 and a primary flow gas of nitrogen or air. The thrust augmentation,  $\phi$ , is defined as  $\phi = T_E / (T_N + J_T)$ , where the ejector thrust,  $T_E$ , is the thrust at the rake location,  $T_N$  is the nozzle thrust, and  $J_T$  is the steady state momentum flux due to the secondary flow in the tunnel.

#### **Calculation of the Ejector Thrust, $T_E$**

The thrust at the rake location,  $T_E$ , is measured using a 17-probe cruciform pitot rake. Centered in the tunnel, the rake has one pitot probe at its center, and four pitot probes, spaced 1.25 in apart, on each of its four arms. At each pitot probe location, the Mach number,  $M$ , is calculated using the Rayleigh supersonic pitot formula and static pressure measurements at the sidewall (see Figure 2). If the rake is upstream of the last sidewall static pressure tap, the static pressure at each rake pitot probe location is found using bilinear interpolation; if the rake is downstream of the last static pressure tap, the static pressure at each pitot probe location is taken to be the static pressure at the last sidewall pressure tap. In other words, interpolation is done but extrapolation is not. After the Mach number is found, the thrust is

found using  $T_E = \frac{1}{\tau} \int_0^\tau \int \gamma p M^2 dA dt$ , where  $\gamma$  is the

ratio of specific heats,  $p$  is the static pressure, and  $\tau$  is the time over which the measurements were taken. The time integral was evaluated using the trapezoid rule, and the area integral was evaluated using the trapezoid rule in polar coordinates.

There are three major sources of uncertainty in the calculation of  $T_E$ . The first is due to the uncertainty in the static pressure at the rake pitot probes,  $\sigma_p$ . To

estimate this uncertainty, the maximum difference,  $d_{\max}$ , between the four sidewall static probes (two on the left sidewall and two on the right sidewall) closest to the rake is first calculated. Since the maximum pressure difference  $d_{\max}$  is usually between pressure taps at different streamwise locations, to find  $\sigma_p$ ,  $d_{\max}$  is multiplied by the factor  $\alpha_p$  and by the ratio of the minimum streamwise distance between the rake and the nearest sidewall pressure tap,  $x_{\min}$ , to the streamwise distance between the two nearest sidewall pressure taps,

$$\Delta x_{sw}: \sigma_p = \left| \alpha_p \frac{x_{\min}}{\Delta x_{sw}} d_{\max} \right|. \text{ If the rake is upstream}$$

of the last sidewall pressure tap (i.e., bilinear interpolation is done), then  $\alpha_p$  is set to 1. If the rake is downstream of the last sidewall static pressure tap (i.e., the static pressure values from the last sidewall static pressure taps are used), then the uncertainty  $\sigma_p$  should be greater than it is when bilinear interpolation can be done, and so  $\alpha_p$  should be greater; it is (somewhat arbitrarily) set to 2. Note that this method is conservative; it should overestimate  $\sigma_p$ .

Once  $\sigma_p$  is known, the uncertainty in the thrust due to the uncertainty in the static pressure,  $\sigma_{T,p}$  can be found using the propagation of errors formula,

$$\sigma_{T,p} = \sigma_p \frac{\partial T_E}{\partial p} \text{ (see, for example Bevington}^8\text{). The}$$

thrust  $T_E$  is calculated using

$$T_E = \frac{1}{\tau} \int_0^{\tau} \int \gamma p [M_E(p, p_{pitot})]^2 dA, \text{ where the Mach}$$

number  $M$  is an implicit function of the static pressure by the Rayleigh pitot formula. Figure 5 (a) shows the derivative of  $T_E$  with respect to static pressure as a function of Mach number. Figure 5 (b) shows the difference in pressure between the last two static taps on the left sidewall of the 1' x 1' supersonic wind tunnel. For each pulse rate, the bar graphs in Figure 5(b) show the percentage of time that the sidewall pressures differed by a given amount for an air case with pulse ring 3 and the rake downstream of the last sidewall pressure tap. Since this difference is usually small,  $\sigma_{T,p}$  is usually less than 5% and always less than 10%.

The other two major causes of uncertainty in the calculation of the ejector thrust  $T_E$  are due to reverse flow in the tunnel ( $\sigma_{T,R}$ ) and to the small number of pitot probes used for this calculation ( $\sigma_{T,\#}$ ). The error  $\sigma_{T,R}$  due to reverse flow in the tunnel should be small. If reverse flow occurs, the pitot pressure will be less than the static pressure at the same location, and thus the rake pitot pressure should be less than the nearest

sidewall static pressures. This only occurs for a small percentage of a pulse in the outer probes of the rake. In addition, due to the unsteady flow, a rake pitot pressure less than the nearest sidewall pressure may not always indicate reverse flow. Instead, it may be due to an expansion wave having reached the rake but not the nearest sidewall pressure tap, or a compression wave having reached the sidewall pressure tap but not the rake. (See, for example, times 0.0095 to 0.01 seconds in Figure 6.) The high speed pressure sensitive paint images, the high speed schlieren images, and the sidewall pressure tap time series all show expansion and compression waves moving upstream and downstream in the tunnel. Thus, the flow may not be reversed even when the pitot pressure is less than a nearby static pressure. The uncertainty  $\sigma_{T,R}$  due to reverse flow in the test section is expected to be small because the area where reverse flow occurs and the time during which it occurs are small. Therefore, it will be neglected in the data reduction.

The uncertainty  $\sigma_{T,\#}$  due to the small number of pitot probes used to calculate  $T_E$  should be similar for all cases for the same primary stream Mach number, and therefore it will also be neglected in this analysis. However, because of neglecting  $\sigma_{T,\#}$  and because of the uncertainty in the calculation of the nozzle thrust (discussed below), the absolute values of the thrust augmentation  $\phi$  will not be accurate. Therefore, when looking at the thrust augmentation results in the next section, it is important to look at the trends rather than at the absolute values of  $\phi$ .

#### Calculation of the Nozzle Thrust, $T_N$

The thrust from the nozzle was not directly measured. Instead, it was calculated using a pitot probe placed at the center of the nozzle exit and a static probe placed at the edge of the nozzle exit (see Figure 7). Since there were often shock or expansion waves between the pitot and static probes (compare Figure 7 and Figure 8), the nozzle exit pressure data was combined with schlieren data for similar cases to find the Mach number and static pressure at the nozzle exit. The Mach number and static pressure exit profiles were assumed to be top hat, so the nozzle thrust  $T_N$  was calculated

$$T_N = \frac{1}{\tau} \int_0^{\tau} \gamma p_N M_N^2 A_N, \text{ where the subscript "N"}$$

indicates conditions at the nozzle exit.

The uncertainty in the thrust from the nozzle is relatively large. When the nozzle is under-expanded, as in Figure 8 (b), the Mach number is determined from measurement of the shock angle. When the nozzle is over-expanded, as in Figure 8 (d), the Mach number is determined by using the measured total and static

pressures at the nozzle exit, the measured shock angle, and a combination of the Rayleigh supersonic pitot formula with the oblique shock relations. At times when the flow is perfectly expanded, or when there is no clear shock or expansion, the Mach number is calculated using measured total and static pressures at the nozzle exit with the Rayleigh supersonic pitot formula. When the nozzle exit flow is subsonic, the isentropic total/static pressure relation is used. The static pressure at the nozzle exit is determined from the total pressure at the nozzle exit using the Rayleigh supersonic pitot formula ( $M_N > 1$ ) or the isentropic total/static pressure relation ( $M_N < 1$ ). Since the schlieren measurements and the nozzle exit pressure measurements come from different runs on different days and the primary and secondary flow conditions were similar but not identical, the uncertainty in the thrust from the nozzle could potentially be relatively large.

In addition, there are large variations in the pitot pressure at the nozzle exit from one pulse to the same point in the next pulse. For the nozzle thrust calculations only, the start of each pulse was computed and the mean pitot pressure at the nozzle exit was ensemble-averaged. At each time during a pulse, the standard deviation of the pitot pressure is computed, and this standard deviation is used to estimate the standard deviation of the nozzle thrust.

After determining the nozzle thrust for several representative cases, a curve fit for nozzle thrust as a function of mean nozzle throat pressure, pulse rate, and static pressure was found. This curve fit was then used to determine the nozzle thrust for all cases.

#### Calculation of the momentum flux due to flow in the tunnel, $J_T$

The momentum flux due to the secondary flow in the tunnel,  $J_T$ , is calculated by  $J_T = \gamma p_T M_T^2 A_T$ , where the subscript "T" indicates conditions in the tunnel immediately before the primary (nozzle) flow was started.

### **RESULTS**

Results for a primary flow gas of air or nitrogen, a primary flow Mach number of 3.7, and a duty cycle of 8% are discussed below. Note that, due to the assumptions made in the calculations, the trends in the thrust augmentation results are more important than the numerical values.

#### Effect of pulse rate and pulse strength

Figure 9 shows that the thrust augmentation increases with increasing pulse rate for all ejector lengths,

secondary flow Mach numbers, and pulse strengths. Since the thrust augmentation of pulsed ejectors is usually greater than that of steady ejectors, as the pulse rate of a pulsed ejector is increased, the thrust augmentation is expected to increase, reach a maximum value, and then decrease to the steady state thrust augmentation value. Therefore, in this experiment, the pulse rate may not yet have reached its optimum value. As the effective pulse rate of an actual pulse detonation engine, with several pulse detonation engine tubes feeding into one ejector, may be well above 120 Hz, the thrust augmentation for an actual pulse detonation engine may be higher than the values seen here.

Figure 9 also shows that as the pulse strength increases, the thrust augmentation increases.

#### Effect of secondary flow Mach number

Figure 10 shows that the thrust augmentation decreases as the secondary flow Mach number increases. This is similar to the results from studies of steady state ejectors that have shown the thrust augmentation decreases as secondary flow Mach number increases.

#### Effect of Ejector Length

To simulate different ejector lengths, the rake (which measured the ejector thrust) was moved to three different locations: 43.31, 44.32, and 46.34 in downstream of the test section entrance (13.81, 14.82, and 16.84 in downstream of the nozzle exit). The ratios  $L/d$  of ejector length to nozzle diameter were 5.72, 6.14, and 6.97. Figure 11 shows the thrust augmentation as a function of rake location for pulse strengths of 300 and 450 psi and several pulse rates at a secondary flow Mach number of 0.3. This figure shows that for the range of ejector lengths studied here, the thrust augmentation is not a strong function of ejector length.

Since previous studies<sup>2,3</sup> have found optimum  $L/d$  ratios in the range of 2 to 3, it is possible that the change in thrust augmentation with ejector length is small because the  $L/d$  ratio is very far from the optimum. However, there are important differences between these studies and the current experiment. Most of the previous studies involved subsonic or mildly supersonic primary flow and no secondary flow. In addition, the ejectors in these nozzles had opened into a plenum before the ejector thrust was measured. In contrast, the current experiment involves highly supersonic primary flow and substantial secondary flow. Unlike the previous studies, in this experiment, the "ejector" (i.e., the supersonic wind tunnel) does not end at the location where the ejector thrust is measured. Therefore, it is also possible that the optimum  $L/d$  location will not be

similar to that found in previous studies. More experiments are needed to determine this.

#### Discussion

The thrust augmentation values obtained in this experiment are well below the values obtained in other experiments[1-4]. There are several possible reasons for the low thrust augmentation values. First, none of the L/d ratios used were probably the optimum L/d ratio. Second, the pulse rates studied all seemed to be below the optimum pulse rate. Third, most previous unsteady ejector studies had no secondary flow; however, as Figure 10 shows, the thrust augmentation decreases dramatically as primary flow Mach number is increased. If L/d and the pulse rate were optimized, the thrust augmentation could increase significantly.

#### SUMMARY

The 1'x1' supersonic wind tunnel at NASA Glenn Research Center was used to simulate a supersonic pulsed ejector. A nozzle mounted in the wind tunnel was used to simulate high speed primary flow, while the tunnel itself simulated an ejector with low speed secondary flow. The primary Mach number, secondary Mach number, duty cycle, pulse rate, primary flow gas, and the location where the thrust augmentation was measured were varied. So far, the data for a primary Mach number of 3.7, secondary flow Mach numbers of 0.2 and 0.3, duty cycle of 8%, pulse rates from 30 to 120 Hz, primary flow gas of air, and ejector thrust measurement locations at L/d of 5.72, 6.14, and 6.97 has been studied. The results show:

- For the pulse rates studied, thrust augmentation increases with increasing pulse rate. The optimum pulse rate is probably greater than 120 Hz. As actual pulse detonation engines may have effective pulse rates well above 120 Hz, the thrust augmentation of actual pulsed ejectors may higher than the values found in this study.

- Thrust augmentation increases with increasing pulse strength.
- The thrust augmentation decreases with increasing secondary flow Mach number.
- The thrust augmentation does not vary much for L/d ratios of 5.7 to 7.

#### REFERENCES

- [1] Lockwood, R.M., "Investigation of the physics of energy transfer from an intermittent jet to an ambient fluid," Hiller Aircraft Corp., ARD-236, 1959.
- [2] Paxson, D.E., Wilson, J., and Dougherty, K.T., "Unsteady ejector performance: an experimental investigation using a pulsejet driver," AIAA 2002-3195, 2002.
- [3] Wilson, J., and Paxson, D.E., "Unsteady ejector performance: an experimental investigation using a resonance tube driver," AIAA 2002-3632, 2002.
- [4] Wilson, J., "A Simple Model of Pulsed Ejector Thrust Augmentation," NASA/CR--2003-212541, 2003.
- [5] Dittmar, J.H., Elliot, D.M., and Horne, Samuel E. III, "The Far Field Noise of a Pulse Detonation Engine," NASA/TM--2003-212307, 2003.
- [6] Fernandez, R., Slater, J.W., and Paxson, D.E., "Pulsed Ejector Wave Propagation Test Program," *Confined Detonations and Pulse Detonation Engines*, Torus Press, Moscow, 2003, pp. 303-326.
- [7] Seablom, K.D., Soeder, R.H., and Stark, D.E., "NASA Glenn 1- by 1-Foot Supersonic Wind Tunnel User Manual," NASA, NASA/TM--1999-208478, 1999.
- [8] Bevington, P.R., "Data Reduction and Error Analysis for the Physical Sciences," McGraw-Hill Book Company, New York, 1969, pp. 336.

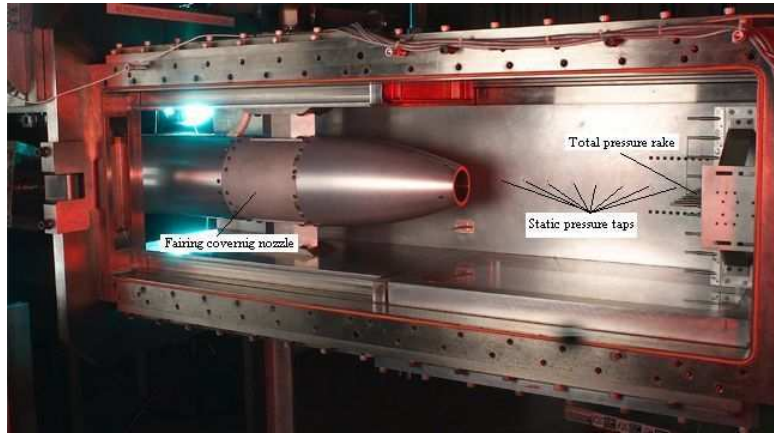


**Figure 1:** Test section of the NASA Glenn 1'x1' supersonic wind tunnel with pulsed ejector equipment installed. Shown are the fairing that covers the Mach 3.7 air nozzle and the total pressure rake. Eight of the sidewall static pressure taps are barely visible.

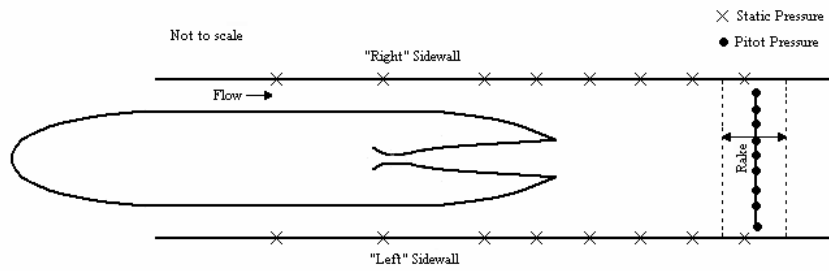


**Figure 2:** Schematic of experimental setup, showing nozzle, nozzle fairing, location of sidewall pressure taps, and rake location.

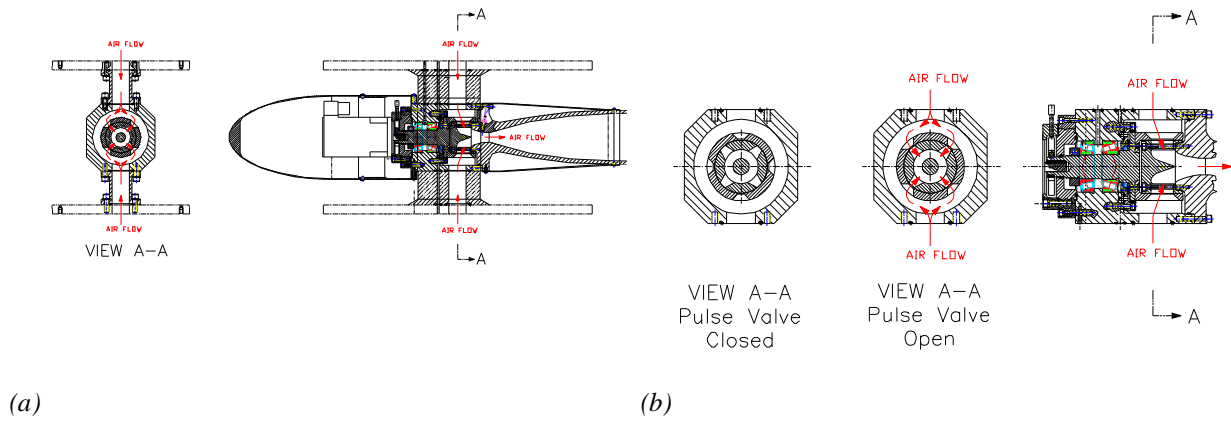


**Figure 3:** Pulse valve mechanism. Part (a) shows cross sectional views of the pulse valve mechanism, motor, exhaust nozzle and wind tunnel walls, while part (b) shows cross sectional views of the pulse valve mechanism in the closed and opened positions.

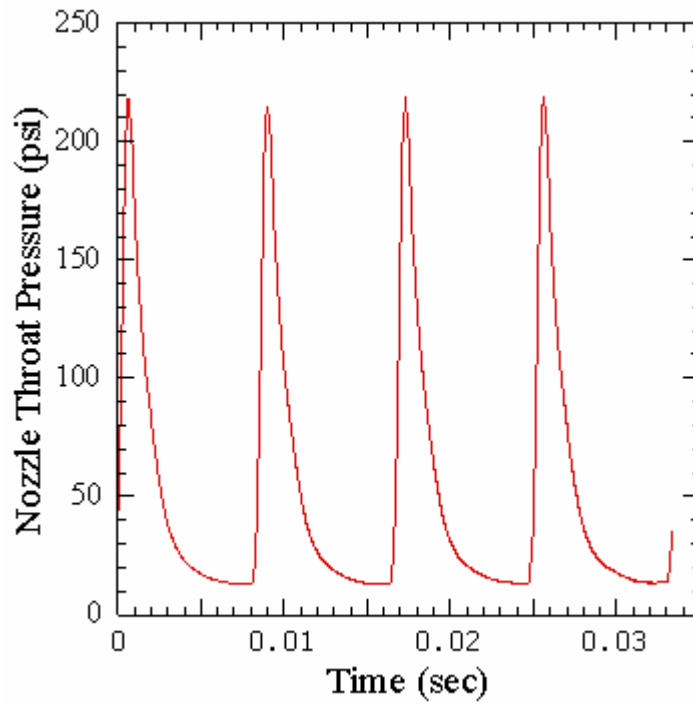
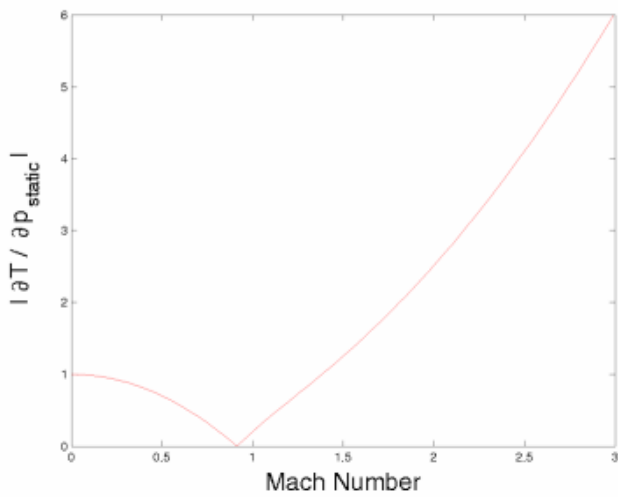
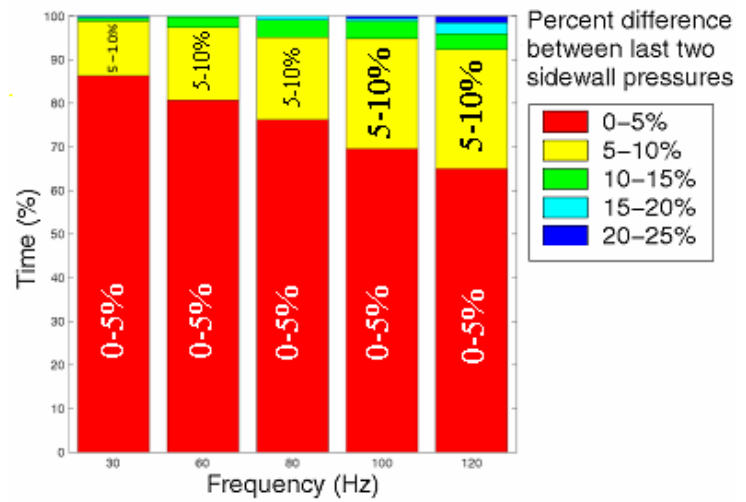


Figure 4: Nozzle throat pressure vs. time for a pulse rate of 120 Hz and a pulse strength of 460 psi.



(a)



(b)

Figure 5: (a) Derivative of thrust with respect to static pressure as a function of Mach number for  $\gamma=1.4$ . (b) Difference between pressures measured by the last two static taps on the left sidewall of the 1'x1' supersonic wind tunnel.

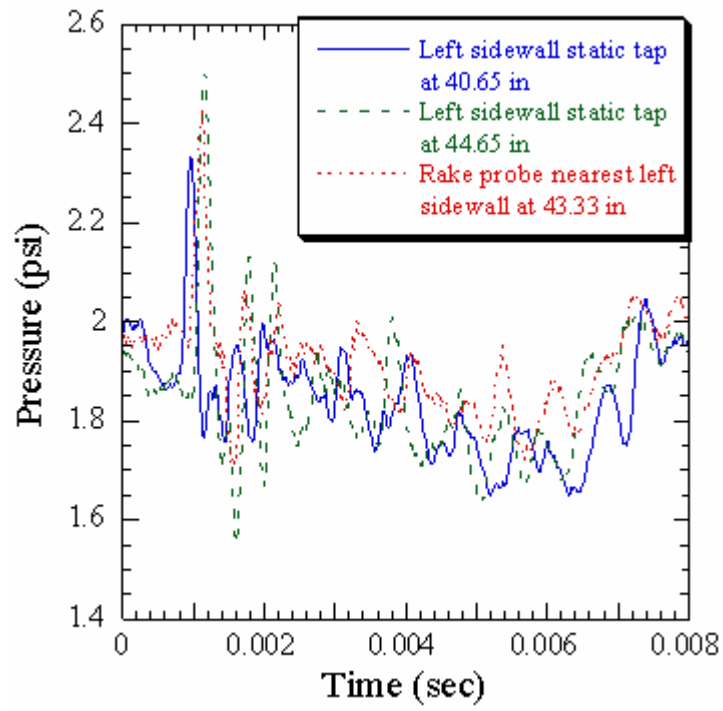
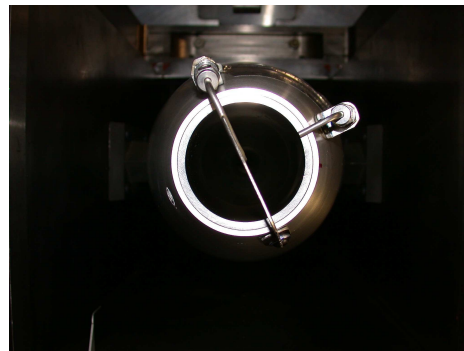
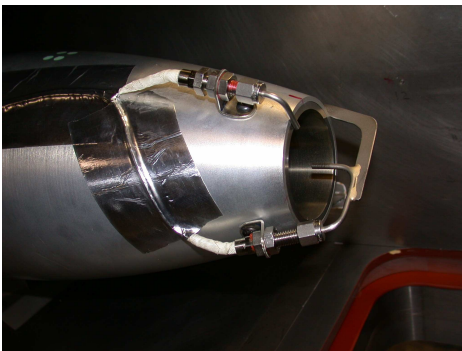
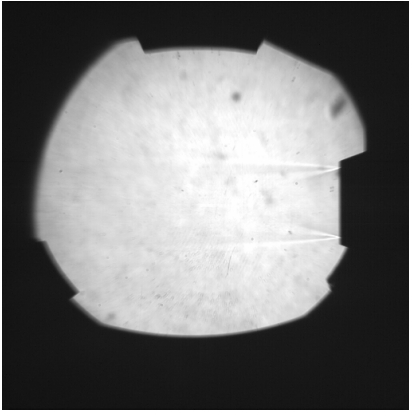


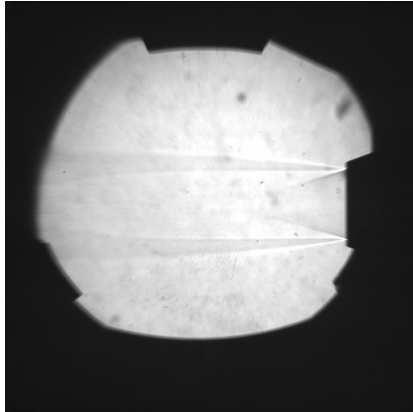
**Figure 6:** Comparison of last two sidewall static pressure taps with the nearest rake pitot pressure for the 120 Hz air case.



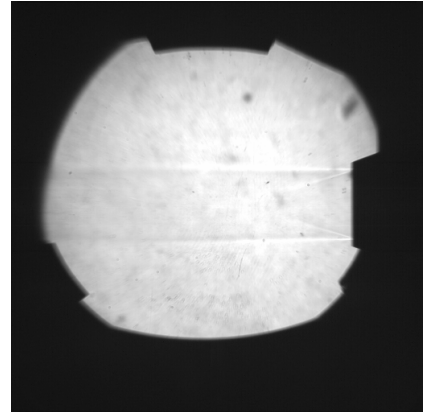
(a) (b)  
**Figure 7:** The pitot and static pressure probes attached to the nozzle exit (on a few runs only) to measure the nozzle thrust.



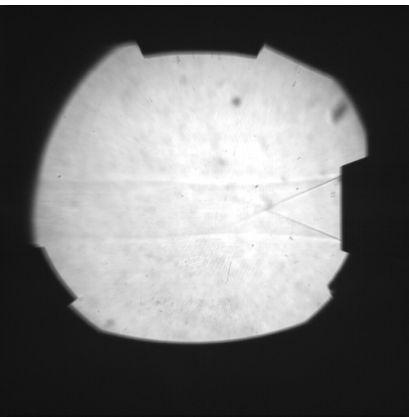
(a)



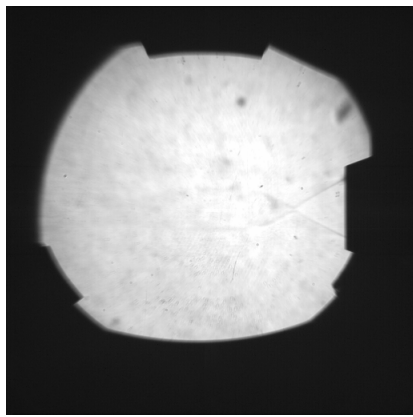
(b)



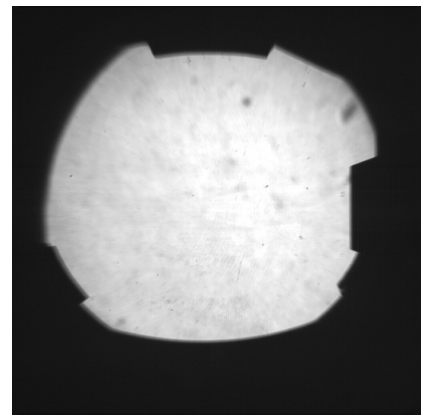
(c)



(d)

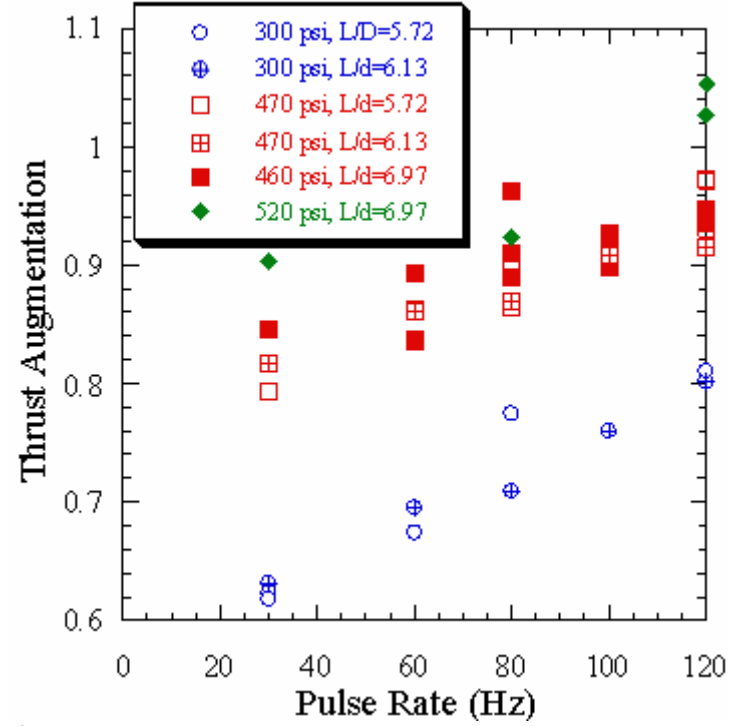
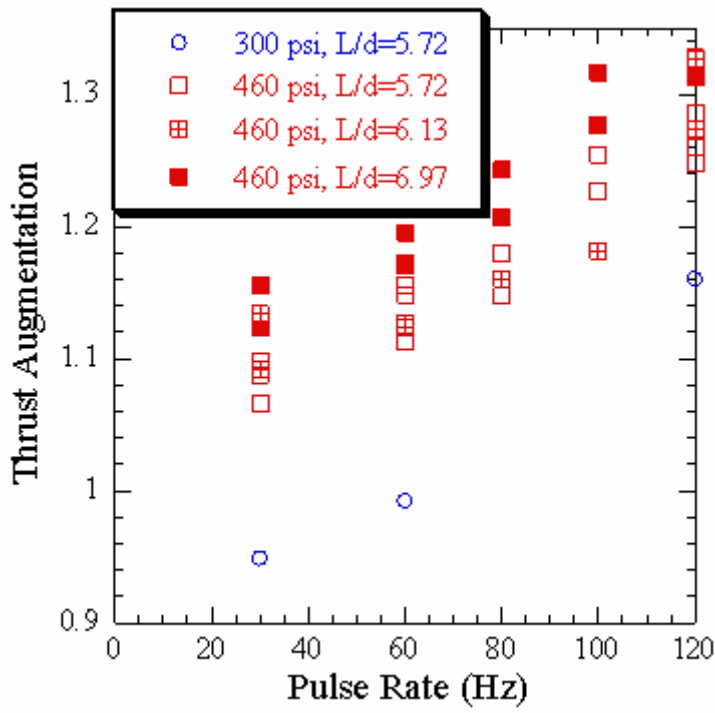


(e)



(f)

**Figure 8:** Typical schlieren images, showing (a) nozzle opening, (b) under-expanded nozzle flow, (c) almost fully expanded nozzle flow, (d) over-expanded nozzle flow, and (e)-(f) nozzle closed.



(a) (b)  
**Figure 9:** Thrust augmentation as a function of pulse rate for a secondary flow Mach number of (a) 0.2 and (b) 0.3.

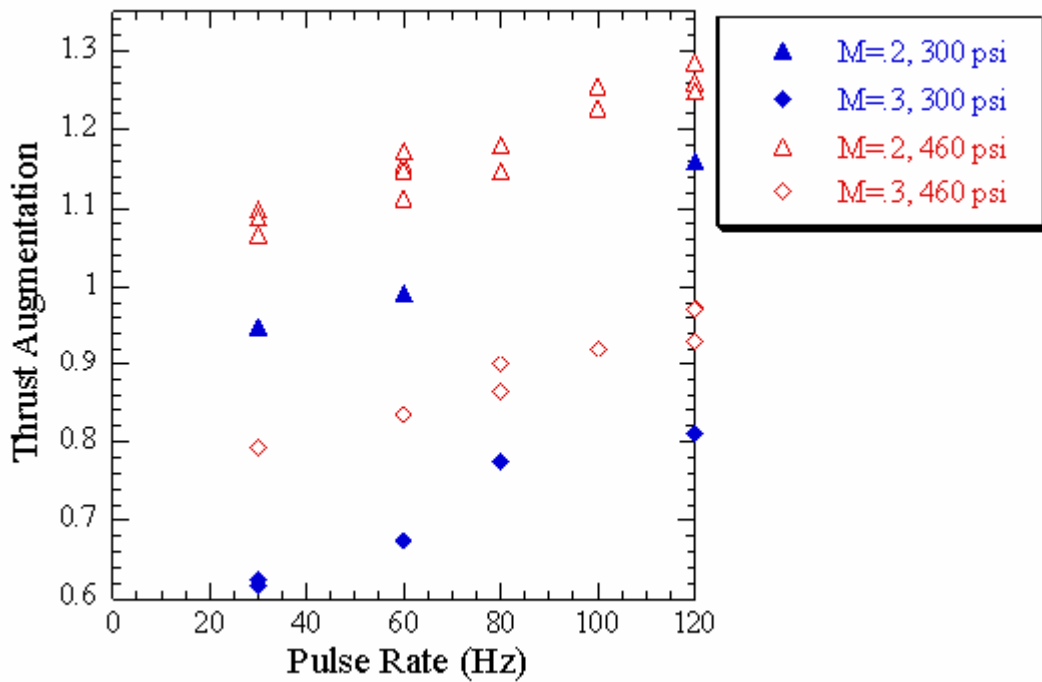
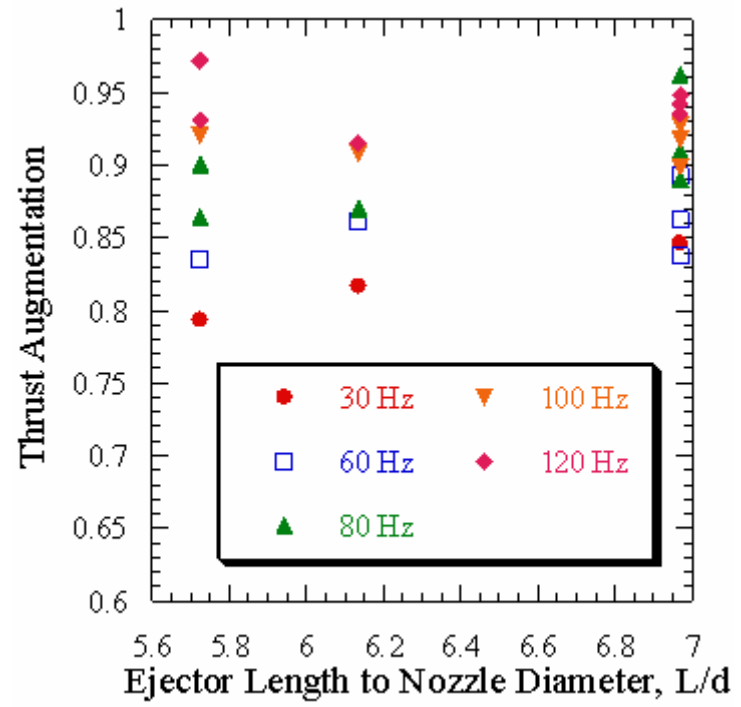
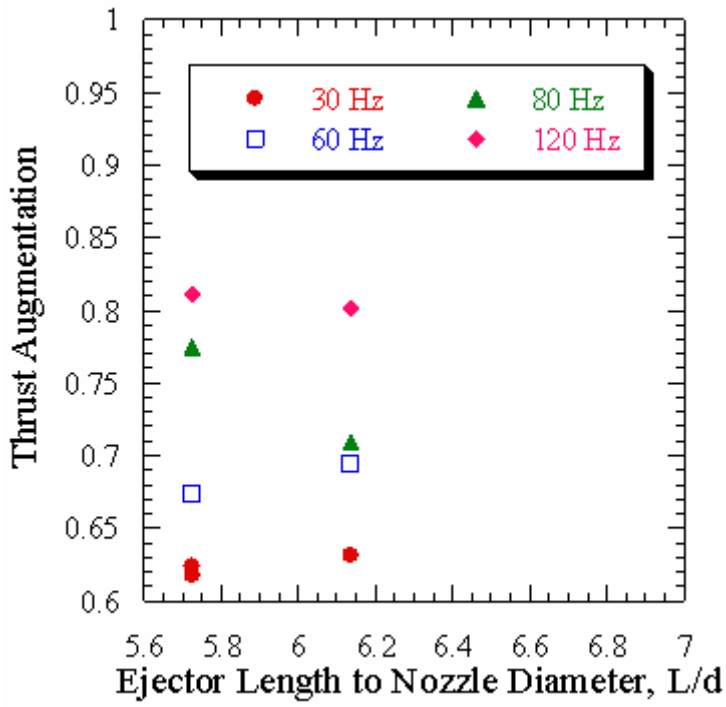


**Figure 10:** Thrust augmentation as at a rake location of  $L/d=5.72$  and a secondary flow Mach numbers of 0.3 and 0.2.



(a)

(b)

**Figure 11** : Thrust augmentation as a function of pulse rate at various rake location for a secondary flow Mach number of 0.3 and a pulse strength of (a) 300 psi and (b) 460 psi.